

## Supporting Information

### **Single atom catalysts supported on N-doped graphene toward fast kinetics in Li–S batteries: a theoretical study**

Xu Han,<sup>a</sup> Zeyun Zhang,<sup>a</sup> and Xuefei Xu<sup>\*a</sup>

<sup>a</sup> *Center for Combustion Energy, Department of Energy and Power Engineering, and Key Laboratory for Thermal Science and Power Engineering of Ministry of Education, Tsinghua University, Beijing 100084, China. E-mail: xuxuefei@tsinghua.edu.cn*

## Contents

1. Optimized structures of $\text{Li}_2\text{S}_m$ on $\text{M@N/G}$	S3–S5
2. Relationships between $G_{\text{ads}}(\text{Li}_2\text{S}_m)$ and $G_{\text{ads}}(\text{S})$ on $\text{M}_{3d}\text{@N/G}$	S6
3. PDOS profiles of S-atom adsorption on Ti, Cr, and $\text{Co@N/G}$	S7
4. Establishment of the descriptor $G_{\text{ads}}(\text{S})$	S8–S10
5. Stability analysis of $\text{M}_{4d,5d}\text{@N4/G}$	S12
6. Prediction of $\Delta G^*_{\text{Li}_2\text{S}_4 \rightarrow \text{Li}_2\text{S}}$ and $\Delta G^{\ddagger}_{\text{dec}}$ on $\text{M}_{4d,5d}\text{@N4/G}$	S11, S13
7. Reasonability of $\Delta G^*_{\text{Li}_2\text{S}_4 \rightarrow \text{Li}_2\text{S}}$ to evaluate discharge kinetics	S14
8. AIMD simulation of $\text{Cr@N4/G}$	S15
9. Stability analysis of $\text{Cr@N4/G}$ and $\text{Mn@N4/G}$ during charge and discharge process	S16
10. Tests of valence states of Mn for Mn-containing systems	S17
11. Values of $G_{\text{ads}}(\text{Li}_2\text{S})$ , $G_{\text{ads}}(\text{Li}_2\text{S}_4)$ , $G_{\text{ads}}(\text{S})$ , $\Delta G^*_{\text{Li}_2\text{S}_4 \rightarrow \text{Li}_2\text{S}}$ , $\Delta G^{\ddagger}_{\text{dec}}$ , $-\text{IpCOHP}$ , $\Delta G_1$ , and $\Delta G_2$ on $\text{M@N/G}$	S18–S22

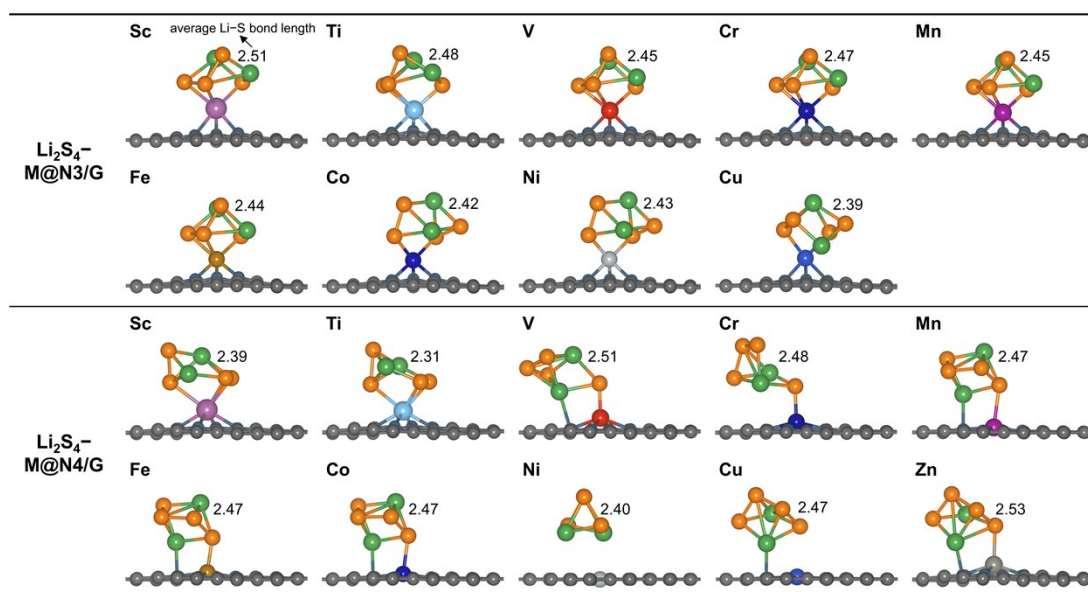


Fig. S1 Optimized adsorption structures of  $\text{Li}_2\text{S}_4$  on  $\text{M}_{3d}\text{@N/G}$ . C, gray; N, blue; Li, green; and S, orange. The numbers given for each structure are average bond lengths of Li-S bonds in Å. Note that there is not a clear relationship between the average lengths of Li-S bonds in the adsorbed  $\text{Li}_2\text{S}_4$  and that of the isolated  $\text{Li}_2\text{S}_4$  molecule (2.51 Å), because not only the lengths of Li-S bonds but also the lengths of S-S bonds would change once the  $\text{Li}_2\text{S}_4$  is adsorbed.

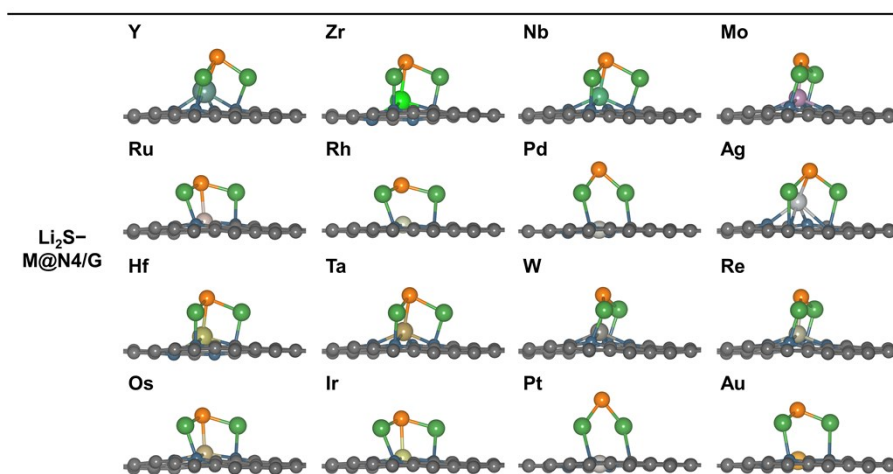


Fig. S2 Optimized adsorption structures of  $\text{Li}_2\text{S}$  on  $\text{M}_{4d,5d}@\text{N}_4/\text{G}$ . C, gray; N, blue; Li, green; and S, orange.

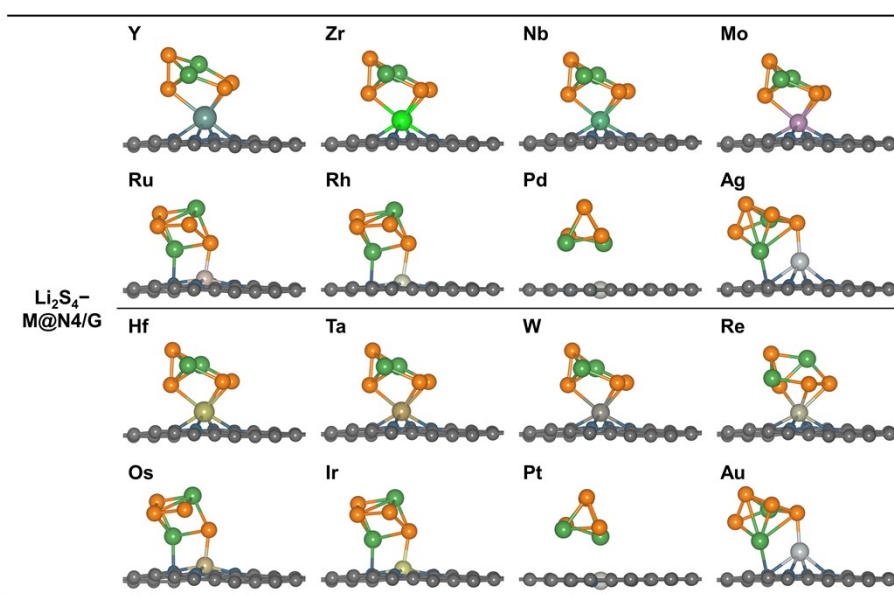


Fig. S3 Optimized adsorption structures of  $\text{Li}_2\text{S}_4$  on  $\text{M}_{4d,5d}@N_4/G$ . C, gray; N, blue; Li, green; and S, orange.

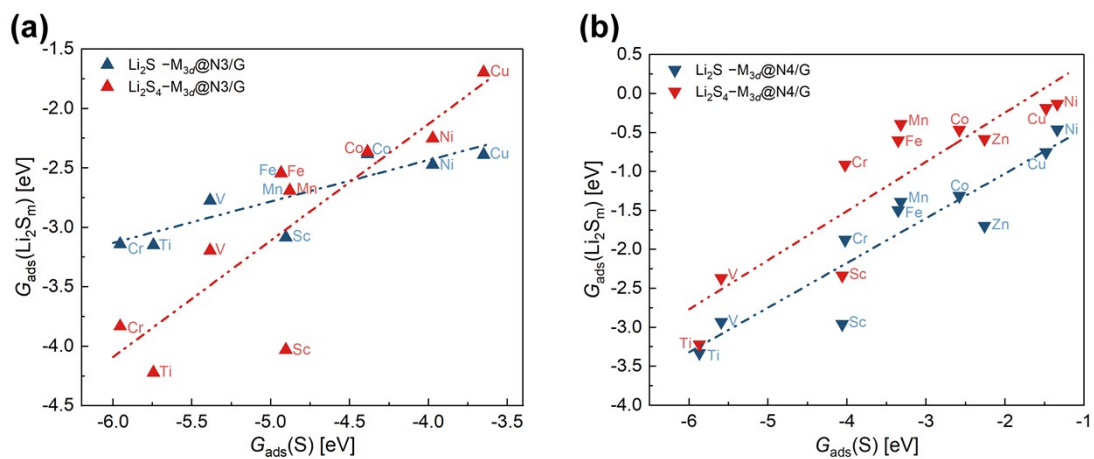


Fig. S4 The relationships about  $G_{\text{ads}}(\text{Li}_2\text{S})$  and  $G_{\text{ads}}(\text{Li}_2\text{S}_4)$  versus  $G_{\text{ads}}(\text{S})$  on (a)  $\text{M}_{3\text{d}}@N3/G$  and (b)  $\text{M}_{3\text{d}}@N4/G$ .

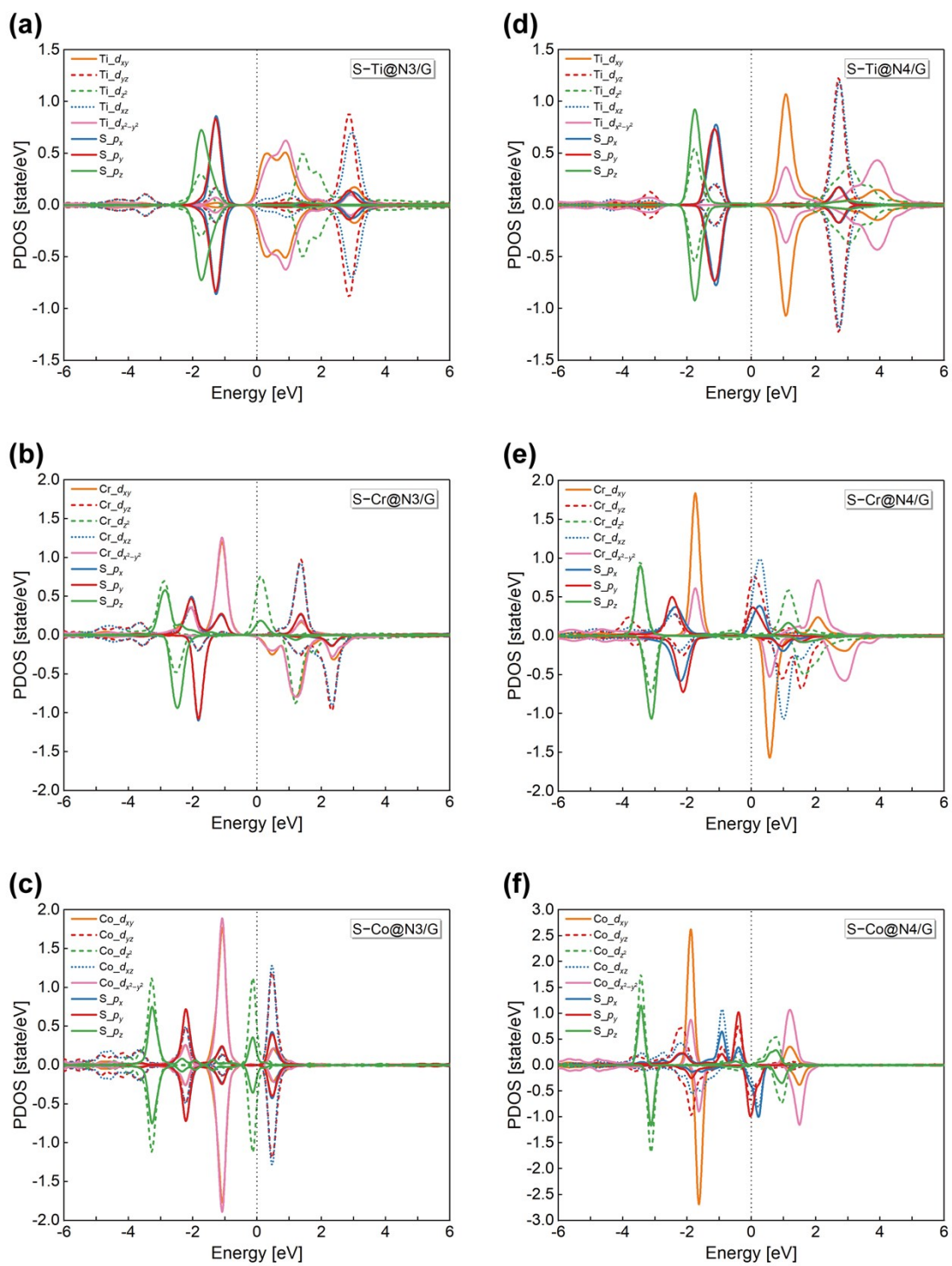


Fig. S5 PDOS profiles of S-atom adsorption on (a) Ti@N3/G, (b) Cr@N3/G, (c) Co@N3/G, (d) Ti@N4/G, (e) Cr@N4/G, and (f) Co@N4/G. The Fermi energy level is set to zero and indicated by the gray dotted line.

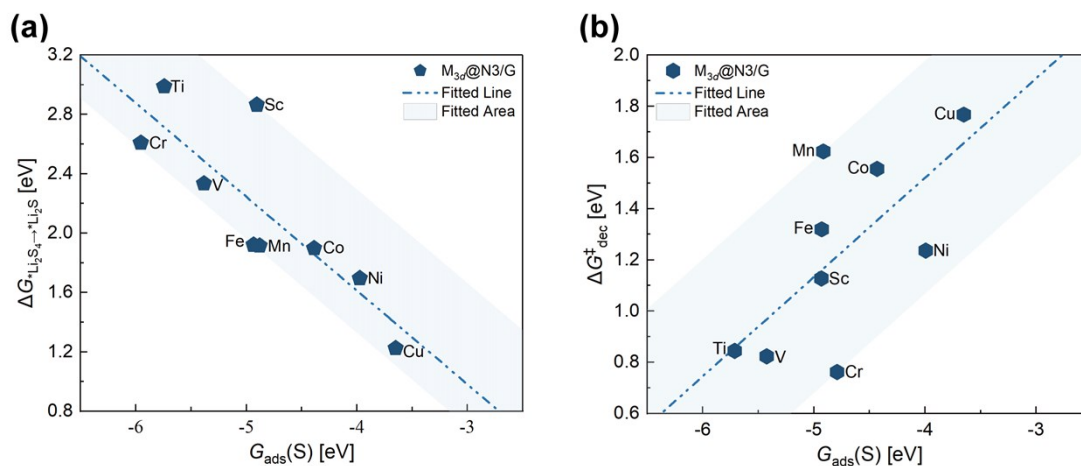


Fig. S6  $G_{\text{ads}}(\text{S})$  versus (a)  $\Delta G^*_{\text{Li}_2\text{S}_4 \rightarrow \text{Li}_2\text{S}}$  and (b)  $\Delta G^{\ddagger}_{\text{dec}}$  on  $M_{3d}@N3/G$ . The symbols are the calculated data. The fitted area is built based on the maximum deviation of data from the fitted line.



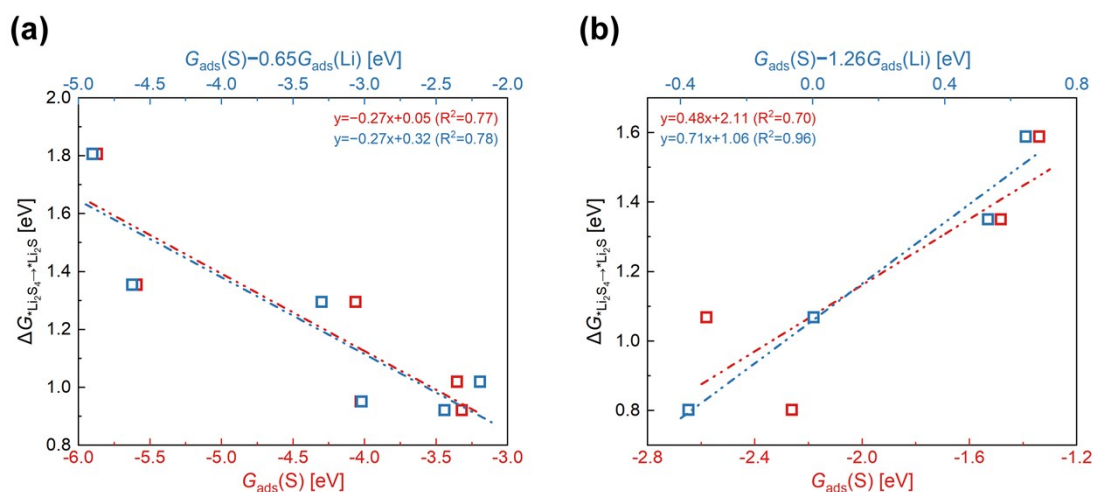


Fig. S7 Comparison of the single descriptor,  $G_{ads}(S)$  (in red), and the double descriptor,  $G_{ads}(S) + \gamma G_{ads}(Li)$  (in blue), versus the  $\Delta G_{*Li_2S_4 \rightarrow *Li_2S}$  on  $M_{3d}@N4/G$ , where (a) is for early  $M_{3d}$  (Sc to Fe) and (b) is for late  $M_{3d}$  (Co to Zn).

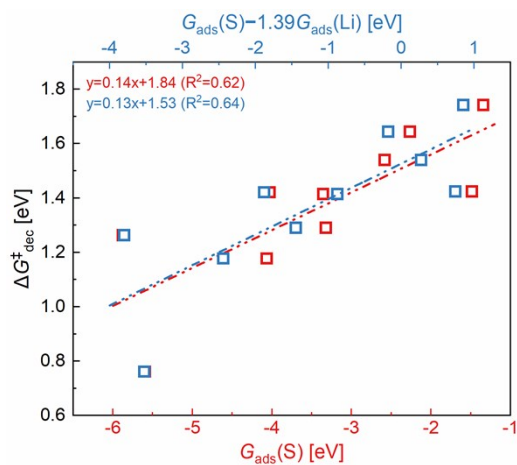


Fig. S8 Comparison of the relationships about the  $\Delta G_{\text{dec}}^{\ddagger}$  on  $\text{M}_{3\text{d}}@\text{N}_4/\text{G}$  versus single descriptor (in red):  $G_{\text{ads}}(\text{S})$ , and double descriptor (in blue):  $G_{\text{ads}}(\text{S}) + \gamma G_{\text{ads}}(\text{Li})$ .

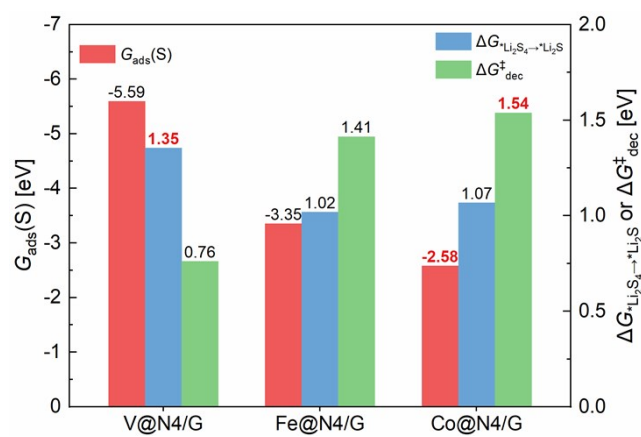


Fig. S9 Our calculated  $G_{\text{ads}}(\text{S})$ ,  $\Delta G_{\text{Li}_2\text{S}_4 \rightarrow \text{Li}_2\text{S}}^*$ ,  $\Delta G_{\text{dec}}^\ddagger$  on the three ever-reported catalysts: V@N4/G, Fe@N4/G, and Co@N4/G.

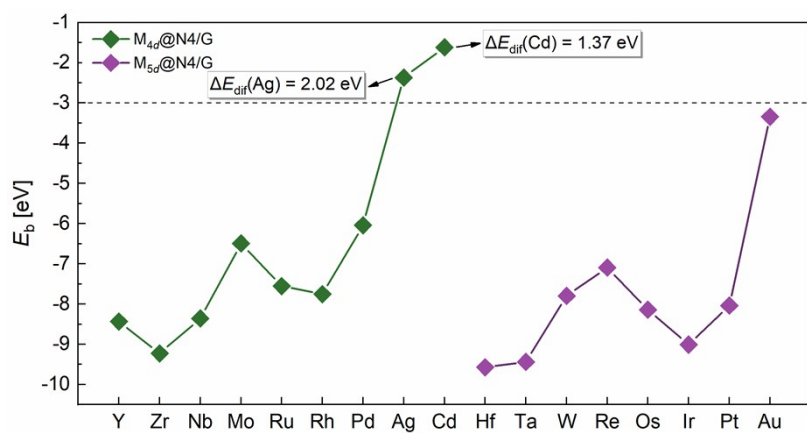


Fig. S10 Binding energies ( $E_b$ ) of  $M_{4d,5d}@N_4/G$ . The values of diffusion energy difference ( $\Delta E_{dif}$ ) of  $Ag@N_4/G$  and  $Cd@N_4/G$  are labeled. The dash line stands for the filter value of  $-3$  eV.

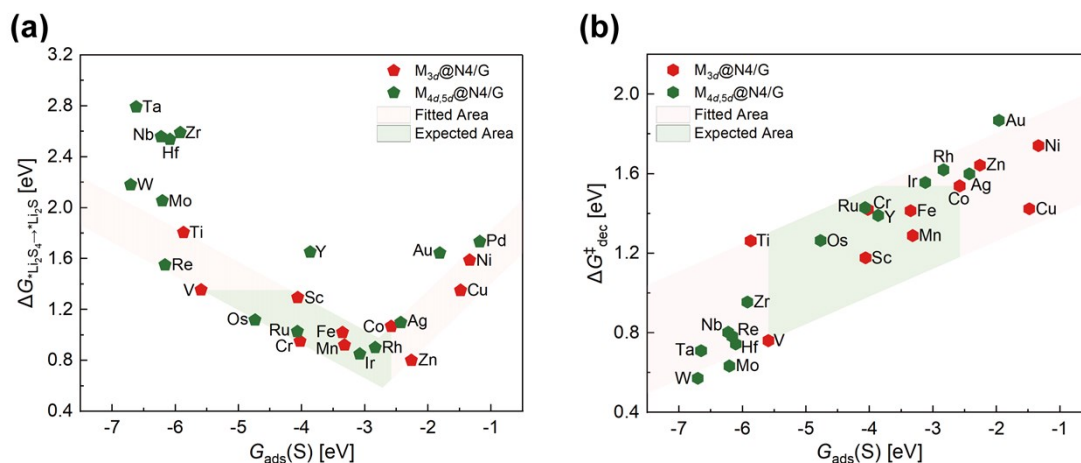


Fig. S11 Relationships between  $G_{\text{ads}}(\text{S})$  and (a)  $\Delta G^*_{\text{Li}_2\text{S}_4 \rightarrow * \text{Li}_2\text{S}}$  and (b)  $\Delta G^*_{\text{dec}}$  on  $M@N4/G$ . The values of  $\text{Pt}@N4/G$  are not marked because of its positive  $G_{\text{ads}}(\text{S})$ , and  $\Delta G^*_{\text{dec}}$  of  $\text{Pd}@N4/G$  is also not given because the stable decomposed structures of  $\text{Li}_2\text{S}$  on it cannot be found.

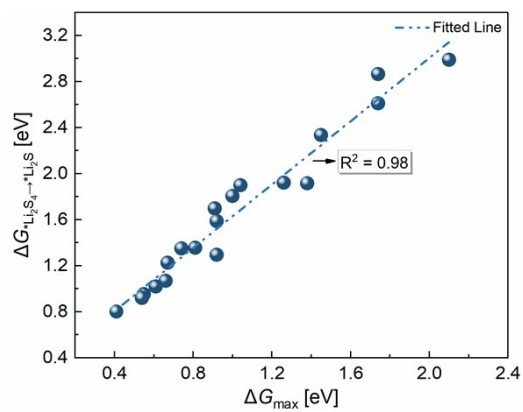


Fig. S12  $\Delta G_{\text{Li}_2\text{S}_4 \rightarrow \text{Li}_2\text{S}}$  versus  $\Delta G_{\max}$  on  $\text{M}_{3\text{d}}@N/G$ .  $\Delta G_{\max}$  is the maximum of the free energy changes of steps R1 and R2.

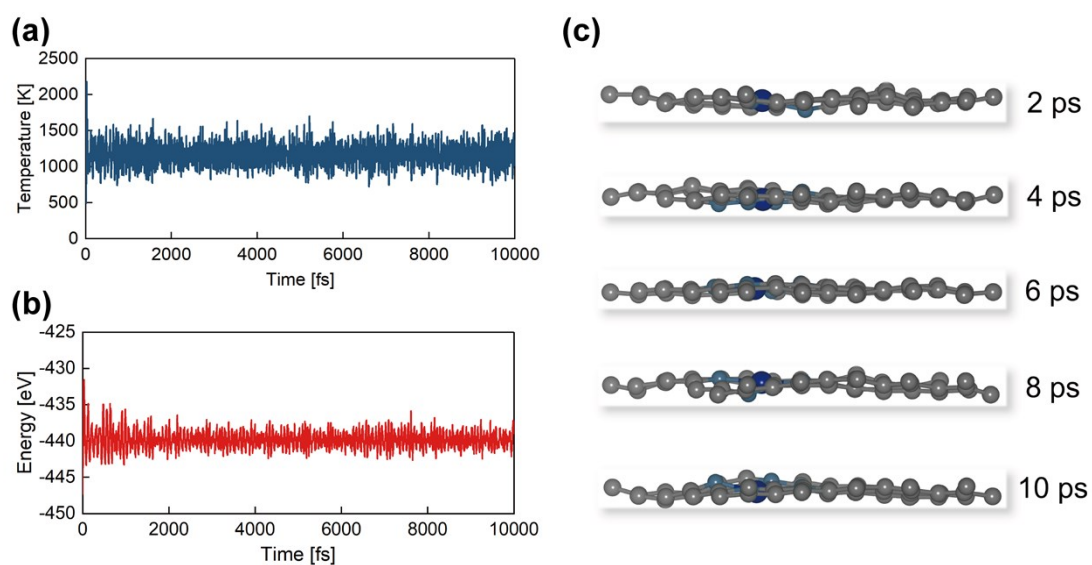


Fig. S13 Variations of (a) temperature and (b) energy over a total time period of 10 ps for the AIMD simulation of Cr@N4/G at 900 °C. (c) Five snapshots of simulated structures of Cr@N4/G at 2 ps, 4 ps, 6 ps, 8 ps, and 10 ps, respectively.

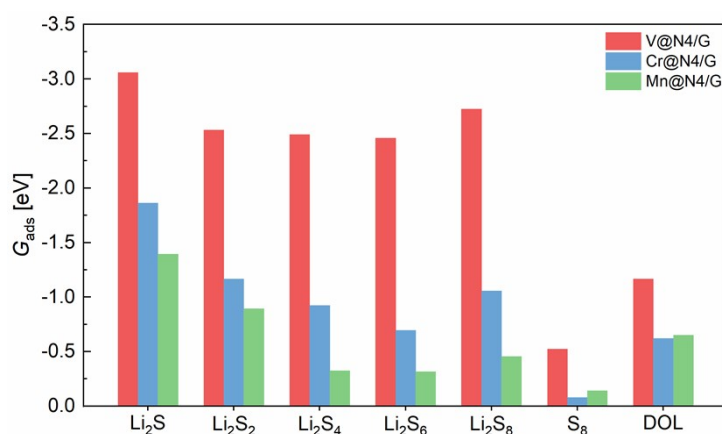


Fig. S14 Comparison of adsorption free energies ( $G_{\text{ads}}$ ) of sulfur species and DOL solvent molecule on V@N4/G, Cr@N4/G, and Mn@N4/G.

### The stability of Cr@N4/G and Mn@N4/G during charge–discharge process

Apart from the feasibility of experimental synthesis, the stability of single atoms (Cr and Mn) during charge–discharge process was also important and should be considered. However, because of expensive computational cost, it is hard to fully (or directly) describe the complex charge–discharge process including the various sulfur species and electrolyte environment. Here we make a reasonable simplification by comparing the interactions of various sulfur species and solvent molecules (we take 1,3-dioxolane (DOL) as an example) with the V, Cr, and Mn@N4/G. The calculated adsorption energies shown in Fig. S14 indicate that sulfur species and DOL all interact more tensely with V@N4/G than with Cr@N4/G and Mn@N4/G. Since V@N4/G has been demonstrated experimentally enough stability working in the system of Li–S batteries,<sup>1</sup><sup>2</sup> we can indirectly conclude that Cr and Mn single atoms can also keep stable on their corresponding M@N4/G framework during charge–discharge process.

<sup>1</sup> Y. Fan, F. Ma, J. Liang, X. Chen, Z. Miao, S. Duan, L. Wang, T. Wang, J. Han, R. Cao, S. Jiao and Q. Li, *Nanoscale*, 2020, **12**, 584–590.

<sup>2</sup> G. Zhou, S. Zhao, T. Wang, S. Z. Yang, B. Johannessen, H. Chen, C. Liu, Y. Ye, Y. Wu, Y. Peng, C. Liu, S. P. Jiang, Q. Zhang and Y. Cui, *Nano Lett.*, 2020, **20**, 1252–1261.



Table S1 Tests of various valence states of transition metals for Mn-containing systems.<sup>a</sup>

System	$M_{\text{test}}$ ( $\mu_B$ )	$M_{\text{opt}}$ ( $\mu_B$ )	$E_{\text{opt}}$ (eV)	$M_{\text{select}}$ ( $\mu_B$ )
Mn@N3/G	0	0	-459.13	5
	1	0	-459.17	
	2	0	-459.17	
	3	5	-459.65	
	4	5	-459.65	
	5	5	-459.65	
Li <sub>2</sub> S-Mn@N3/G	0	2	-470.49	5
	1	0	-470.23	
	2	0	-470.23	
	3	5	-471.00	
	4	5	-471.00	
	5	5	-471.00	
Li <sub>2</sub> S <sub>4</sub> -Mn@N3/G	0	1	-485.34	3
	1	3	-485.88	
	2	3	-485.88	
	3	3	-485.88	
	4	3	-485.88	
	5	3	-485.88	
Mn@N4/G	0	3	-451.71	3
	1	0	-450.40	
	2	3	-451.71	
	3	3	-451.71	
	4	3	-451.71	
	5	3	-451.71	
Li <sub>2</sub> S-Mn@N4/G	0	0	-461.46	2
	1	2	-461.83	
	2	2	-461.83	
	3	2	-461.83	
	4	2	-461.83	
	5	2	-461.83	
Li <sub>2</sub> S <sub>4</sub> -Mn@N4/G	0	0	-475.10	3
	1	0	-475.10	
	2	3	-475.53	
	3	3	-475.53	
	4	3	-475.53	
	5	3	-475.53	

<sup>a</sup>In this table,  $M_{\text{test}}$  and  $M_{\text{opt}}$  are the magnetic moments of input structures and optimized structures, respectively.  $E_{\text{opt}}$  denote the energies of optimized structures and  $M_{\text{select}}$  denote the final-determined magnetic moments for further investigations.

Table S2 Calculated  $G_{\text{ads}}(\text{Li}_2\text{S})$ ,  $G_{\text{ads}}(\text{Li}_2\text{S}_4)$ ,  $G_{\text{ads}}(\text{S})$ ,  $\Delta G^*_{\text{Li}_2\text{S}_4 \rightarrow \text{Li}_2\text{S}}$ , and  $\Delta G^*_{\text{dec}}$  (in eV) on M@N/G.

Support	M	$G_{\text{ads}}(\text{Li}_2\text{S})$	$G_{\text{ads}}(\text{Li}_2\text{S}_4)$	$G_{\text{ads}}(\text{S})$	$\Delta G^*_{\text{Li}_2\text{S}_4 \rightarrow \text{Li}_2\text{S}}$	$\Delta G^*_{\text{dec}}$
M@N3/G	Sc	-3.08	-4.03	-4.90	2.86	1.13
	Ti	-3.15	-4.22	-5.74	2.99	0.84
	V	-2.77	-3.19	-5.38	2.33	0.82
	Cr	-3.14	-3.83	-5.95	2.61	0.76
	Mn	-2.69	-2.69	-4.88	1.92	1.62
	Fe	-2.54	-2.55	-4.93	1.92	1.32
	Co	-2.38	-2.36	-4.39	1.90	1.56
	Ni	-2.47	-2.25	-3.97	1.70	1.24
	Cu	-2.39	-1.70	-3.65	1.22	1.77
M@N4/G	Sc	-2.96	-2.34	-4.06	1.29	1.18
	Ti	-3.33	-3.22	-5.87	1.81	1.26
	V	-2.93	-2.37	-5.59	1.35	0.76
	Cr	-1.88	-0.91	-4.03	0.95	1.42
	Mn	-1.39	-0.39	-3.32	0.92	1.29
	Fe	-1.50	-0.60	-3.35	1.02	1.41
	Co	-1.31	-0.47	-2.58	1.07	1.54
	Ni	-0.46	-0.13	-1.34	1.59	1.74
	Cu	-0.75	-0.19	-1.48	1.35	1.42
	Zn	-1.70	-0.58	-2.26	0.80	1.64
	Y	-2.75	-2.48	-3.86	1.65	1.39
	Zr	-3.49	-4.16	-5.92	2.59	0.95
	Nb	-3.37	-4.01	-6.23	2.56	0.80
	Mo	-3.12	-3.26	-6.21	2.05	0.63
	Ru	-2.41	-1.52	-4.07	1.03	1.43
Rh	-1.50	-0.48	-2.83	0.90	1.62	
Pd	-0.35	-0.17	-1.18	1.73	N/A	

	Ag	-1.93	-1.11	-2.43	1.10	1.60
	Hf	-3.63	-4.25	-6.11	2.54	0.74
	Ta	-3.51	-4.38	-6.65	2.79	0.71
	W	-3.36	-3.63	-6.70	2.18	0.57
M@N4/G	Re	-3.12	-2.75	-6.16	1.55	0.78
	Os	-2.50	-1.70	-4.77	1.12	1.26
	Ir	-1.53	-0.46	-3.12	0.85	1.56
	Pt	0.27	0.37	0.10	N/A	N/A
	Au	-0.29	-0.02	-1.96	1.64	1.87

---

Table S3 Calculated  $-IpCOHP$  of different atom pairs between adsorbed  $Li_2S$  or  $Li_2S_4$  and  $M_{3d}@N/G$ .

Support	Adsorbate	M	Atom pair					
			S-M	Li-N	Li-C	S-N	S-C	Li-M
M@N3/G	Li <sub>2</sub> S	Sc	2.29	0.45	0.43	0	0	0
		Ti	2.50	1.03	0.56	0	0	0.02
		V	2.24	1.15	0.50	0	0	-0.03
		Cr	2.89	0.59	0.40	0	0	0.24
		Mn	2.37	0.58	0.39	0	0	0.28
		Fe	2.49	0.50	0.39	0	0	0.22
		Co	2.42	0.81	0.31	0	0	0.30
		Ni	2.36	0.69	0.32	0	0	0.34
		Cu	1.96	0.66	0.30	0	0	0.31
M@N3/G	Li <sub>2</sub> S <sub>4</sub>	Sc	1.88	0	0	0	0	0
		Ti	1.83	0	0	0	0	0
		V	1.51	0	0	0	0	0
		Cr	2.12	0	0	0	0	0
		Mn	2.02	0	0	0	0	0.30
		Fe	1.94	0.35	0	0.09	0	0.29
		Co	2.80	0	0	0.16	0	0.30
M@N4/G	Li <sub>2</sub> S	Ni	2.48	0	0	0.21	0	0.29
		Cu	1.80	0.42	0.37	0	0	0.30
		Sc	2.54	1.03	0.42	0	0	0.01
		Ti	2.82	1.32	0.53	0	0	0.01
		V	2.65	1.41	0.49	0	0	-0.05
		Cr	2.71	0.95	0.31	0	0	0.23
		Mn	2.34	1.00	0.33	0	0	0.22
Fe	1.99	0.96	0.33	0	0	0.23		
Co	1.38	0.91	0.34	0	0	0.21		
Ni	0.27	0.89	0.29	0	0	0.21		

		Cu	1.16	0.88	0.35	0	0	0.23
		Zn	1.46	0.91	0.30	0	0	0.35
		Sc	1.48	0	0	0.15	0	0
		Ti	1.61	0	0	0.32	0	0
		V	3.23	1.10	0.54	0	0	0.28
		Cr	2.50	0.90	0.27	0	0	0.21
		Mn	0.91	0.90	0.26	0	0	0.21
M@N4/G	Li <sub>2</sub> S <sub>4</sub>	Fe	2.65	0.94	0.30	0.17	0	0.24
		Co	1.29	0.89	0.26	0	0	0.21
		Ni	0	0	0.21	0	0	0.33
		Cu	0	0.69	0.31	0	0	0.19
		Zn	1.17	0.67	0.38	0	0	0.34

Table S4 Calculated free energy changes (in eV) for step R1 ( $\Delta G_1$ ) and step R2 ( $\Delta G_2$ ).<sup>a</sup>

Support	M3	$\Delta G_1$	$\Delta G_2$
M@N3/G	Sc	<b>1.74</b> <sup>b</sup>	1.13
	Ti	<b>2.10</b>	0.89
	V	<b>1.45</b>	0.89
	Cr	<b>1.74</b>	0.86
	Mn	<b>1.38</b>	0.53
	Fe	<b>1.26</b>	0.66
	Co	0.86	<b>1.04</b>
	Ni	<b>0.91</b>	0.79
	Cu	0.55	<b>0.67</b>
M@N4/G	Sc	0.37	<b>0.92</b>
	Ti	<b>1.00</b>	0.80
	V	0.55	<b>0.81</b>
	Cr	0.40	<b>0.55</b>
	Mn	<b>0.54</b>	0.38
	Fe	<b>0.61</b>	0.41
	Co	<b>0.66</b>	0.41
	Ni	<b>0.92</b>	0.67
	Cu	<b>0.74</b>	0.61
Zn	<b>0.41</b>	0.39	

<sup>a</sup> R1:  $^*Li_2S_2 \rightarrow ^*Li_2S + (1/8) S_8$ ; R2:  $^*Li_2S_4 \rightarrow ^*Li_2S_2 + (1/4)S_8$ .

<sup>b</sup> The maximum ( $\Delta G_{max}$ ) of  $\Delta G_1$  and  $\Delta G_2$  is bold, corresponding to the rate-determining step.